Acta Crystallographica Section F
Structural Biology and Crystallization Communications
ISSN 1744-3091

In-house SIRAS phasing of the polyunsaturated fatty-acid isomerase from *Propionibacterium acnes*

Alena Liavonchanka,[a] Ellen Hornung,[a] Ivo Feussner[a] and Markus Rudolph[b]*

[a]Department of Plant Biochemistry, Georg-August-Universität, Justus-von-Liebig Weg 11, 37077 Göttingen, Germany, and [b]Department of Molecular Structural Biology, Institute for Microbiology and Genetics, Georg-August-Universität, Justus-von-Liebig Weg 11, 37077 Göttingen, Germany

Correspondence e-mail: mrudolp2@gwdg.de

Received 21 November 2005
Accepted 11 January 2006

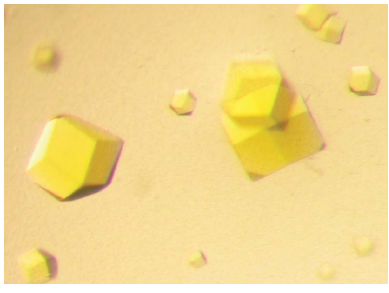

The polyenoic fatty-acid isomerase from *Propionibacterium acnes* (PAI) catalyzes the double-bond isomerization of linoleic acid to conjugated linoleic acid, which is a dairy- or meat-derived fatty acid in the human diet. PAI was overproduced in *Escherichia coli* and purified to homogeneity as a yellow-coloured protein. The nature of the bound cofactor was analyzed by absorption and fluorescence spectroscopy. Single crystals of PAI were obtained in two crystal forms. Cubic shaped crystals belong to space group $I2_13$, with a unit-cell parameter of 160.4 Å, and plate-like crystals belong to the monoclinic space group $C2$, with unit-cell parameters a = 133.7, b = 60.8, c = 72.2 Å, β = 115.8°. Both crystal forms contain one molecule per asymmetric unit and diffract to a resolution of better than 2.0 Å. Initial phases were obtained by SIRAS from in-house data from a cubic crystal that was soaked with an unusually low KI concentration of 0.25 *M*.

1. Introduction

Conjugated linoleic acid (CLA) is a collective term for positional and geometric isomers of linoleic acid (9-*cis*,12-*cis* octadecadienoic acid). Two isomers, 9-*cis*,11-*trans* and 10-*trans*,12-*cis* CLA, have been shown to exert anti-carcinogenic, anti-atherogenic, anti-obesity, anti-inflammatory and antidiabetic effects in mammals (Choi *et al.*, 2001). The main source of CLA in the human diet is meat and milk from ruminants and these essential fatty acids can be limiting. Commercial food enrichment with CLA relies on the chemical isomerization of plant oils rich in linoleic acid (LA), which yields several isomers in an ill-defined mixture. As it has been shown that individual CLA isomers have different effects *in vivo* (Wahle *et al.*, 2004), an alternative and more specific route for CLA production would be *via* enzymatic isomerization of easily accessible precursors.

To this end, the gene coding for the *Propionibacterium acnes* polyenoic fatty-acid isomerase (PAI; EMBL accession code q6a8x5) has been cloned, the protein recombinantly produced in *Escherichia coli* and its biochemical properties assessed (Hornung *et al.*, 2006). PAI catalyzes the isomerization of LA to 10-*trans*,12-*cis* CLA, but also accepts other C18 fatty acids such as linolenic (6-*cis*,9-*cis*, 12-*cis* octatrienoic) acid as substrates. Two other polyenoic fatty-acid isomerases from *Butyrivibrio fibrisolvens* (Kepler *et al.*, 1970, 1971) and the algae *Ptilota filicina* (Sanders *et al.*, 2001; Zheng *et al.*, 2002) have been described. The algal enzyme does not share significant sequence homology with PAI and there is no sequence information for the *Butyrivibrio* enzyme. In addition, no structure of any fatty-acid isomerase is available. With the aim of obtaining a structural description of the polyenoic fatty-acid isomerization reaction, we have crystallized PAI in two forms and employed halide-based phasing to generate initial electron-density maps. Furthermore, we initially characterized by absorption and fluorescence spectroscopy a yellow-coloured cofactor, probably a flavin, which is likely to be involved in catalysis.

2. Methods

2.1. Protein purification and spectroscopic procedures

PAI was cloned from genomic DNA of *P. acnes* and overproduced in *E. coli* as described by Hornung *et al.* (2006). Purification of PAI

will be described in detail elsewhere (Liavonchanka *et al.*, 2006). Absorption spectra of 40 µ*M* solutions of FAD and PAI were recorded at room temperature in 50 m*M* Tris–HCl pH 7.5 on a single-beam Xe-flashlamp absorption spectrometer (Fig. 1*a*). Fluorescence emission spectra in the range 460–650 nm (10 nm bandwidth) were measured at 298 K on a FluoroMax3 spectrofluorimeter at 2 µ*M* (FAD) and 6 µ*M* (PAI) concentrations in 40 m*M* sodium phosphate pH 7.5 after excitation at 450 nm (1 nm bandwidth) and an integration time of 1 s (Fig. 1*b*).

2.2. Crystallization and crystal characterization

Initial PAI crystals of irregular shape were obtained from condition No. 39 of Crystal Screen I (Hampton Research), *i.e.* 0.1 *M* HEPES–NaOH pH 7.5, 2 *M* $(NH_4)_2SO_4$, 2%(*v*/*v*) PEG 400 at 283 K using a protein concentration of 5 mg ml^{-1} by sitting-drop vapour diffusion. Based on this lead condition, cubic shaped crystals of PAI were grown by mixing equal volumes of 10 mg ml^{-1} PAI with 0.1 *M* Tris–HCl pH 8.5, 2 *M* Li_2SO_4 and either 2%(*v*/*v*) PEG 400 or 2%(*v*/*v*) 1,4-butanediol (Fig. 1*c*). Plate-like crystals grew from 0.1 *M* MES–NaOH

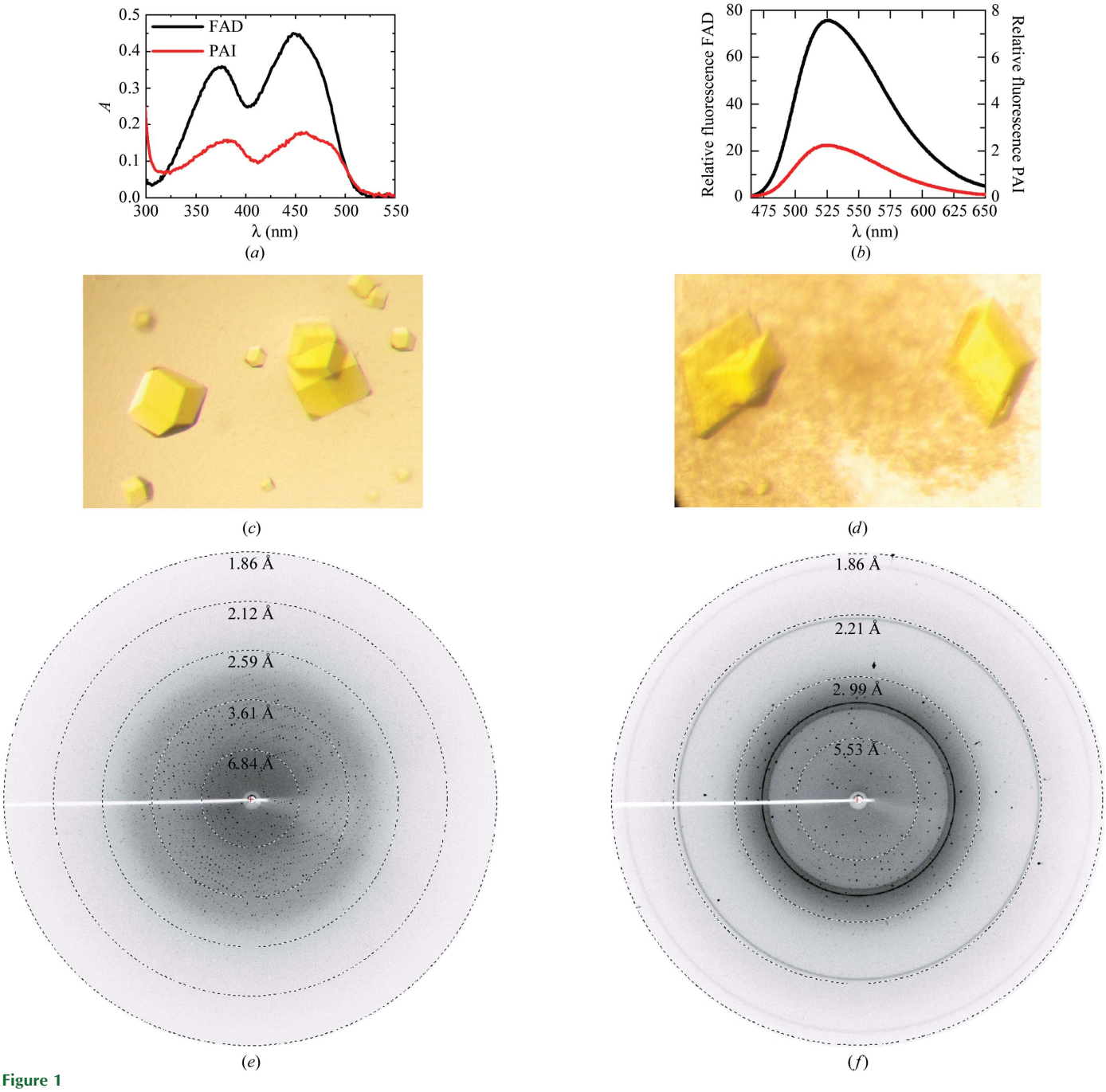

Figure 1
Analysis of the cofactor and crystallization of PAI. (*a*) UV spectra of 40 µ*M* solutions of free FAD (black curve) and PAI (red curve) show the two characteristic absorption maxima for an oxidized flavin (FAD or FMN) at 360–390 nm and 440–470 nm. (*b*) The fluorescence emission spectra of free FAD (2 µ*M*, black curve) and PAI (6 µ*M*, red curve) show the characteristic flavin emission at 525 nm. Cofactor fluorescence is strongly quenched when bound to the protein (compare second ordinate). (*c*) Cubic PAI crystals from 0.1 *M* Tris–HCl pH 8.5, 2 *M* Li_2SO_4, 2%(*v*/*v*) PEG 400. (*d*) Monoclinic PAI crystals from 0.1 *M* MES–NaOH pH 6.0, 2 *M* $(NH_4)_2SO_4$, 5%(*v*/*v*) PEG 400. The longest dimension in both crystal forms is 0.2 mm. (*e*) and (*f*) show diffraction patterns of the cubic and monoclinic crystals, respectively, collected in-house on a MAR345 imaging-plate detector at a distance of 150 mm after 10 min exposure. The outer resolution is 1.86 Å.

pH 6.0, 2 *M* $(NH_4)_2SO_4$, 5%(*v*/*v*) PEG 400 (Fig. 1*d*). The cubic crystals were directly cryocooled in liquid nitrogen without additional cryoprotectant, while plates were cryoprotected in mother liquor supplemented with 12.5%(*v*/*v*) PEG 400. Crystals were mounted in an arbitrary orientation and data were collected in-house on a MAR345dtb image-plate detector mounted on a MicroMax 007 generator operating with a copper target. The exposure time was 10 min, the oscillation angle was 0.5° and the crystal-to-detector was distance 150 mm. Data reduction was performed with the *HKL* suite of programs (Otwinowski & Minor, 1997) (Table 1). Indexing of the diffraction pattern of the cubic crystals (Fig. 1*e*) was consistent with space groups *I*23 or $I2_13$, which cannot be distinguished based on systematic absences. The diffraction pattern of the plate-shaped crystals (Fig. 1*f*) indexed in monoclinic space group *C*2. There is one molecule per asymmetric unit in both crystal forms.

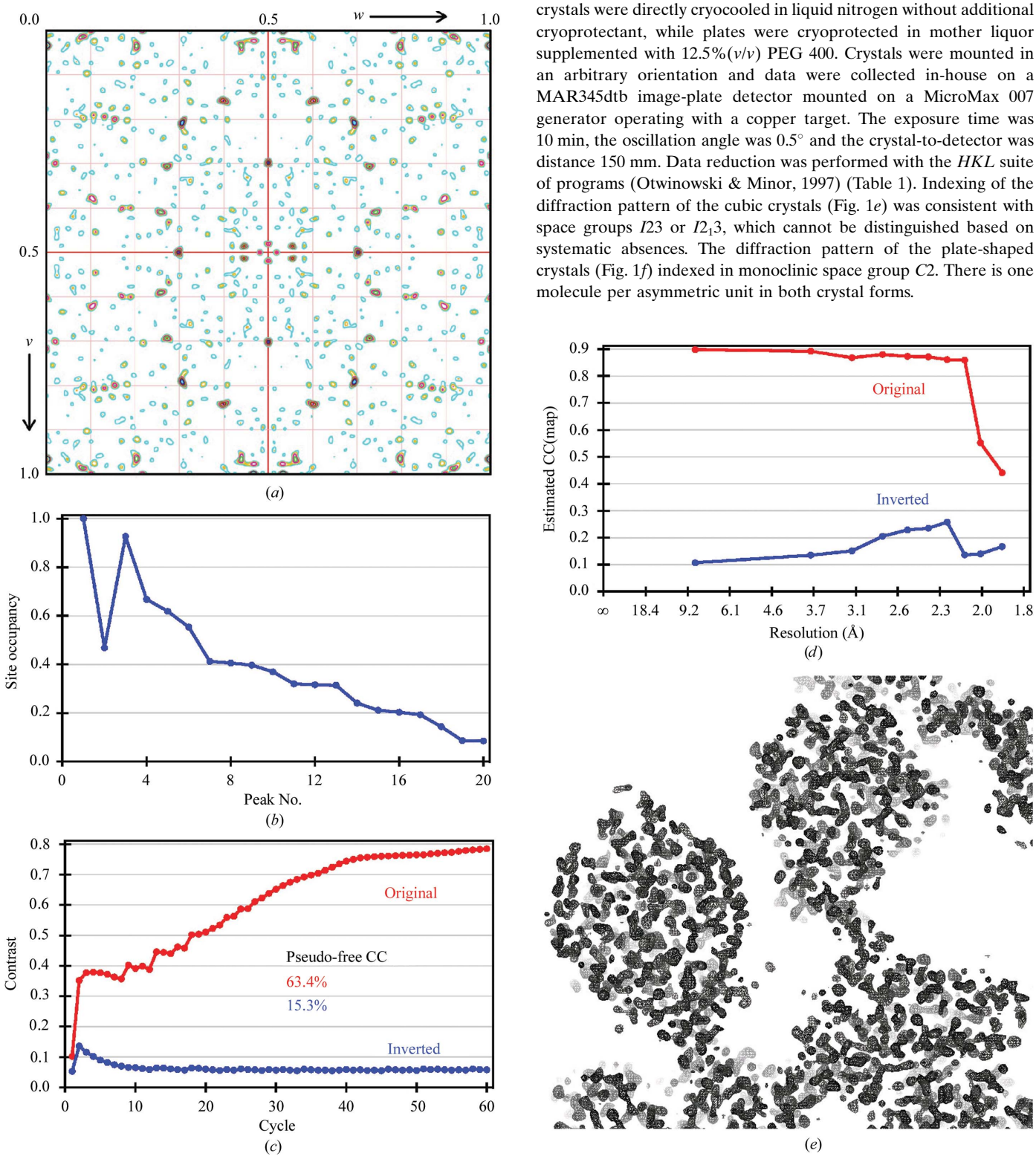

Figure 2
SIRAS phasing of cubic PAI. (*a*) Anomalous difference Patterson map at section $u = 0.5$ calculated to a resolution of 3 Å showing several distinct peaks for bound iodide. Contours are in steps of 1σ and are coloured differently for each level. (*b*) Graphical representation of Table 2 showing a drop in occupancy to ~0.2 at site No. 14. Iodide 2 is located on a crystallographic twofold. The top 13 sites were used as input for density modification and enantiomer selection in *SHELXE*. (*c*) Progress of density modification and phase extension monitored by the protein/solvent contrast *versus* modification cycle. While the correct hand of the substructure is immediately apparent, the quality of the electron density requires at least 60 cycles for convergence. (*d*) Estimated map correlation coefficient as a function of resolution calculated with density-modified phases. (*b*), (*c*) and (*d*) were generated with *HKL2MAP* (Pape & Schneider, 2004). (*e*) Experimental electron-density map contoured at 2.0σ after density modification and phase extension in *SHELXE*. The 30 Å section encompasses three molecules and shows a clear solvent boundary.

Table 1
X-ray data-collection statistics.

Values in parentheses are for data in the highest resolution shell (2.00–1.95 Å for the native data sets and 2.29–2.21 Å for the KI soak).

Data set	Native I	KI soak	Native II
Space group	$I2_13$	$I2_13$	$C2$
Unit-cell parameters (Å, °)	a = 160.4	a = 160.3	a = 133.7, b = 60.8, c = 72.2, β = 115.8
Matthews coefficient (Å^3 Da^{-1})	3.7	3.7	2.8
Solvent content (%)	65	65	55
Wavelength (Å)	1.54	1.54	1.54
Resolution range (Å)	50–1.95	50–2.21	50–1.95
Unique reflections	49143	58536	37527
Completeness (%)	98.4 (78.2)	87.9 (19.7)	100 (98.1)
Mean $I/\sigma(I)$	14.0 (1.3)	12.1 (1.0)	11.4 (2.5)
$R_{\rm merge}$†	9.9 (75.6)	12.9 (55.5)	12.3 (61.2)

† $R_{\rm merge} = \sum_{hkl}\sum_i |I_{hkl} - \langle I_{hkl}\rangle|/\sum_{hkl}\sum_i I_{hkl}$.

Table 2
Fractional coordinates of the ten most occupied iodide sites as determined by *SHELXD*.

Site	x	y	z	Occupancy
1	0.232	0.101	0.250	1.00
2	0.250	0.112	0.500	0.47
3	0.356	0.153	0.448	0.93
4	0.167	0.022	0.128	0.67
5	0.163	0.074	0.050	0.62
6	0.370	0.209	0.456	0.55
7	0.124	0.039	−0.046	0.41
8	0.213	0.006	0.220	0.41
9	0.381	0.067	0.478	0.40
10	0.158	0.021	0.211	0.37

3. Results and discussion

3.1. Spectroscopic characterization of the yellow cofactor

Upon concentration, it was noticed that PAI is yellow in colour. Protein aggregation can lead to yellow colouring owing to light scattering, but no such scattering was observed in absorption measurements and PAI eluted in a monodisperse form from a gel-filtration column (data not shown). Thus, a cofactor of the flavin type or an iron cluster could be present in PAI. The absorption spectrum of PAI in the 300–500 nm range shows two bands at 370 and 460 nm (Fig. 1*a*) indicative of the isoalloxazine ring of an oxidized flavin. A control measurement with FAD seconded this hypothesis. Flavins also fluoresce at 525 nm after excitation at 450 nm (Chapman & Reid, 1999). Typical flavin fluorescence was found when the emission spectra of FAD and PAI were compared (Fig. 1*b*). Upon binding of flavins to proteins, their fluorescence is strongly quenched (Chapman & Reid, 1999), which is also the case for PAI. The maximal fluorescence emission intensity of PAI is >80-fold lower than that of free FAD. Taken together, these spectroscopic data indicate the presence of a flavin, FAD or FMN, in PAI, which is likely to function as a cofactor in fatty-acid isomerization.

3.2. In-house SIRAS phasing after halide soaking

Halide soaking is a potentially rapid method for either in-house (using iodide) or synchrotron (using bromide) phasing by SAD or SIRAS (Dauter *et al.*, 2000). The high symmetry ($I23$ or $I2_13$) and solvent content (65%) of the cubic crystal form are beneficial factors for density modification once a halide substructure has been found. Crystals were briefly (<1 min) soaked in mother liquor supplemented with 1.0 *M* KI, but tended to crack and failed to diffract X-rays. As halides weakly and non-covalently bind to both ionic and hydrophobic areas of the protein surface, high concentrations of >0.5 *M* of the halide salt are usually used (Uson *et al.*, 2003). Exceptions are lysozyme and xylanase, where 0.35 and 0.5 *M* KI were used, respectively (Dauter *et al.*, 2000). In the case of PAI, the highest KI concentration that still retained crystal morphology and diffraction (Table 1) was 0.25 *M*, which might result in reduced occupancy of the derivative sites. An anomalous difference Patterson map at Harker section u = 0.5 calculated to 3 Å resolution with the origin removed showed a number of significant peaks >10σ, indicating successful derivatization (Fig. 2*a*). Analysis for anomalous signal content with *SHELXC* by comparing the anomalous signal-to-noise ratio based on the variances of F^+ and F^- revealed $\Delta F/\sigma(\Delta F)$ ratios of >1.16 for reflections of <3.5 Å resolution, where a value of 0.8 indicates no anomalous signal (Zwart, 2005). Substructure-determination calculations were performed with *SHELXD* (Schneider & Sheldrick, 2002) using data truncated at a resolution of 3.5 Å in space groups $I23$ and $I2_13$. A SAD experiment in space group $I2_13$ resulted in a 14-atom substructure with occupancies >0.2 (correlation coefficient CC of 0.47/0.26 for all/weak reflections). This substructure yielded interpretable electron-density maps after a quite extensive density-modification and phase-extension scheme of 300 cycles in *SHELXE* (estimated map CC of 0.85 to 2.5 Å resolution; data not shown) and also established the space group as $I2_13$.

A higher quality substructure solution was obtained in a SIRAS experiment against data set native I (Table 1). The derived substructure of 13 sites with relative occupancy >0.2 had a CC of 0.51 and 0.39 for all and for weak reflections, respectively (Fig. 2*b* and Table 2). Density modification and phase extension using this substructure immediately established the correct hand of the substructure, but required at least 60 cycles to converge at the maximum protein/solvent contrast (Fig. 2*c*). Electron density calculated with these phases had an overall estimated map CC of 0.85 to 2.2 Å resolution (Fig. 2*d*) and showed a clear solvent boundary (Fig. 2*e*).

This work was supported by the Deutsche Forschungsgemeinschaft (SFB 523; TP A16 to MGR). AL is supported by IMPRS Molecular Biology, Göttingen, Germany.

References

Chapman, S. K. & Reid, G. A. (1999). *Methods Mol. Biol.* **131**, 27–28.
Choi, Y., Park, Y., Pariza, M. W. & Ntambi, J. M. (2001). *Biochem. Biophys. Res. Commun.* **284**, 689–693.
Dauter, Z., Dauter, M. & Rajashankar, K. R. (2000). *Acta Cryst.* D**56**, 232–237.
Hornung, E., Krueger, C., Pernstich, C., Gipmans, M., Porzel, A. & Feussner, I. (2006). In the press.
Kepler, C. R., Tucker, W. P. & Tove, S. B. (1970). *J. Biol. Chem.* **245**, 3612–3620.
Kepler, C. R., Tucker, W. P. & Tove, S. B. (1971). *J. Biol. Chem.* **246**, 2765–2771.
Liavonchanka, A., Hornung, E., Feussner, I. & Rudolph, M. G. (2006). In the press.
Otwinowski, Z. & Minor, W. (1997). *Methods Enzymol.* **276**, 307–326.
Pape, T. & Schneider, T. R. (2004). *J. Appl. Cryst.* **37**, 843–844.
Sanders, D. A., Staines, A. G., McMahon, S. A., McNeil, M. R., Whitfield, C. & Naismith, J. H. (2001). *Nature Struct. Biol.* **8**, 858–863.
Schneider, T. R. & Sheldrick, G. M. (2002). *Acta Cryst.* D**58**, 1772–1779.
Usón, I., Schmidt, B., von Bulow, R., Grimme, S., von Figura, K., Dauter, M., Rajashankar, K. R., Dauter, Z. & Sheldrick, G. M. (2003). *Acta Cryst.* D**59**, 57–66.
Wahle, K. W., Heys, S. D. & Rotondo, D. (2004). *Prog. Lipid Res.* **43**, 553–587.
Zheng, W., Wise, M. L., Wyrick, A., Metz, J. G., Yuan, L. & Gerwick, W. H. (2002). *Arch. Biochem. Biophys.* **401**, 11–20.
Zwart, P. H. (2005). *Acta Cryst.* D**61**, 1437–1448.